JOURNAL OF CATALYSIS 49, 51–82 (1977)

Surface Morphology of Platinum Catalysts[1]

M. FLYTZANI-STEPHANOPOULOS, S. WONG,[2] AND L. D. SCHMIDT

Department of Chemical Engineering and Materials Science, University of Minnesota, Minneapolis, Minnesota 55455

Received February 1, 1977

Surface morphologies of small (<0.06 cm diameter) single crystal spheres of Pt and other transition metals are examined using scanning electron microscopy (SEM) following their use as catalysts in NH_3, C_3H_8, and CO oxidation reactions and in NH_3 decomposition at a total pressure of 1 atm. The stabilities of all regions of the stereographic triangle are examined from SEM micrographs and reflectance patterns, and relative areas of planes are estimated.

Between one and five stable crystal planes are observed for these reactions, and the planes formed and their relative areas depend strongly on the reaction and reactant composition. Unstable planes break up into facets of these planes, but smooth curved regions and pits are observed under certain conditions.

Dependences on time, temperature, sphere diameter, and flow velocity are examined for NH_3 oxidation. It is found that the rate of facet formation is larger on small spheres and that the stable planes and their relative areas are influenced by both sphere diameter and flow velocity. Facet dimensions are 1 to 5 μm for all reactions under most conditions, and facet size increases slowly with reaction time. It is shown that metal transport by either surface diffusion or volatile oxide formation is possible in most cases and that minimum surface free energy considerations can account for unstable and metastable regions and faceting rates. Boundary layer influences on metal transport and the dependence of etching on sphere diameter and flow velocity are also considered.

INTRODUCTION

At the operating temperatures and over the lifetimes of most catalysts, they are in a dynamic state with respect to surface morphology and crystal size. This is observed directly as roughening and metal loss on low area gauze catalysts and is inferred from sintering and dispersion processes on metal crystallites supported on porous oxides. It has been frequently noted (*1–4*) that the presence of gases and surface reactions can greatly enhance these processes, and it is reasonable to suspect that many activation and deactivation processes of catalysts may arise from alterations in surface morphology produced by reaction.

To assess the role of changing surface morphology in surface reaction rates and to apply single crystal plane rate measurements to real catalysts, the planes exposed on catalysts and their relative areas are needed. Some time ago, Gwathmey and co-workers (*5–7*) used large (~1 cm diameter) single crystal spheres to study facet patterns and reactions on Ni and Cu using replication and transmission electron microscopy to observe structures. However, this elegant method does not appear to have been utilized extensively within the last 20 years.

[1] This work partially supported by NSF under Grant No. ENG75-01918.

[2] Present address: Department of Chemical Engineering, Northwestern University, Evanston, Ill. 60201.

ISSN 0021-9517

We have used small (0.01–0.1 cm diameter) single crystal spheres of Pt and other noble metals to examine the structures formed in several catalytic reactions at a total pressure of 1 atm. Spheres of this size are readily prepared by torch melting of wires, crystallographic orientation can be determined by symmetry of etch patterns, and a single sphere reveals the morphology of all surface orientations. We have observed the planes formed versus reaction, gas composition, flow rate, surface temperature, and sphere diameter. Many observations are necessarily qualitative, but it is possible from these measurements to determine semiquantitatively the relative areas of crystal planes on catalyst surfaces.

EXPERIMENTAL METHODS

Single crystal spheres were prepared by melting the ends of high purity (99.9+%) Pt, Pd, Rh, and alloy wires. Spheres were melted either in a CH_4–O_2 torch in air or by electron bombardment heating in vacuum. All spheres shown here were on 0.0025–0.025 cm diameter wires and all were torch melted. Typically 6–8 spheres were prepared simultaneously by spot-welding their wires to a 0.025 cm diameter Pt wire which could be heated resistively in the reactor to ignite the reaction or to attain temperatures above the adiabatic temperature. A SEM micrograph of a typical wire is shown in Fig. 1b.

The reactor was a Pyrex tube 2 cm in diameter through which gases passed at measured flow rates. High purity gases (>99.9%) were used, and feed lines were passed through liquid nitrogen or dry ice for cryogenic purification in some cases. Sphere temperatures were measured with an optical pyrometer for $T > 900$ K and by resistance thermometry for lower temperatures. Temperatures are regarded as accurate to within ± 50 K. Operating conditions in CO oxidation and C_3H_8 oxidation were limited to low temperatures and specific compositions by explosion limits for these reactions.

Wires were removed from the reactor for examination in either a Cambridge Instruments or Ultrascan SEM which had resolutions between 200 and 1000 Å. Typically only about one-half of the spheres were single crystals. Some had large holes from the melting process and some were heavily covered with noncrystalline foreign material. No photographs of these spheres are shown, but imperfect specimens essentially always displayed the same structures as more perfect spheres shown here.

TABLE 1

Relative Areas of Pt Sphere Catalysts

Plane	Annealed	NH_3 oxidation					NH_3 decomposition 22 hr	C_3H_8 oxidation 2% C_3H_8, 2 hr	CO oxidation 50% CO, 2 hr
		5% NH_3 5 hr	10% NH_3 5 hr	20% NH_3 5 hr	50% NH_3 5 hr	10% NH_3 high flow			
(111)	0.075	0.31	0.23	0.18	0.21	0.14	0.11	0.52	0.20
(100)	0.005	0.54	0.08	0.12	0.10	0.86	0.12	0.48	0.16
(110)	—	0.15	0.21	0.16	0.16	—	—	—	—
(210)	—	—	—	0.14	0.18	—	—	—	—
(211)	—	—	—	—	0.35	—	—	—	—
(421)	—	—	0.48	0.40	—	—	0.75	—	—
(310)	—	—	—	—	—	—	—	—	0.64
Curved	0.920	—	—	—	—	—	0.02	—	—

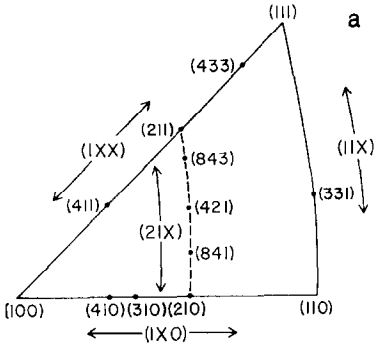

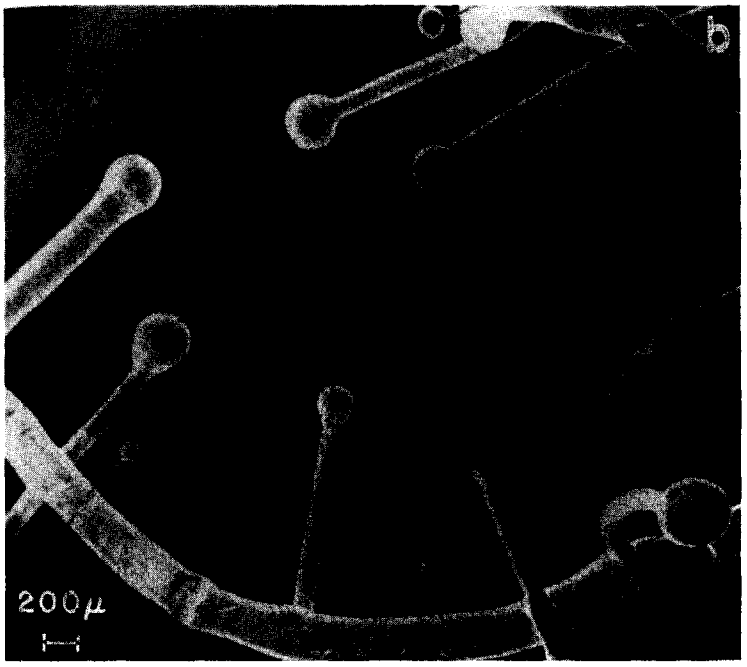

FIG. 1a. Stereographic triangle showing locations of planes and zones referred to in the text. (b) SEM micrograph showing typical spheres, their support wires, and the 0.025 cm diameter wire by which spheres were mounted and heated resistively. (c) Single crystal sphere before being used as a catalyst. The {111} and {100} planes are flat, but the rest of the surface is smooth and curved. (d) Reflectance patterns of the region near the {100} plane from a sphere used in 10% NH_3 oxidation. (e) and (f) Micrographs of various regions of a 0.03 cm diameter sphere used in oxidation of 10% NH_3 in air after 5 hr at 1100 K. (e) Complete sphere; (f) detail showing flat {421} planes.

Figure 1c shows a sphere before reaction. It exhibits flat {111} and smaller {100} planes but the rest of the surface is nearly spherical. Table 1 shows the fractions of {111}, {100}, and curved regions on this surface. This shape indicated that these spheres probably possess their high temperature equilibrium form (*8*) since the observed flat areas are consistent with minimum surface free energy, and the spherical curved regions outside the flats are in agreement with theory for temperatures near the melting point. From the real diameters of the flat planes and the radius of the crystal the surface energy of the flat area $\{hkl\}$ relative to the curved surface energy $\bar{\gamma}$ of the metal can be calculated (*8*).

Figure 1a shows the stereographic tri-

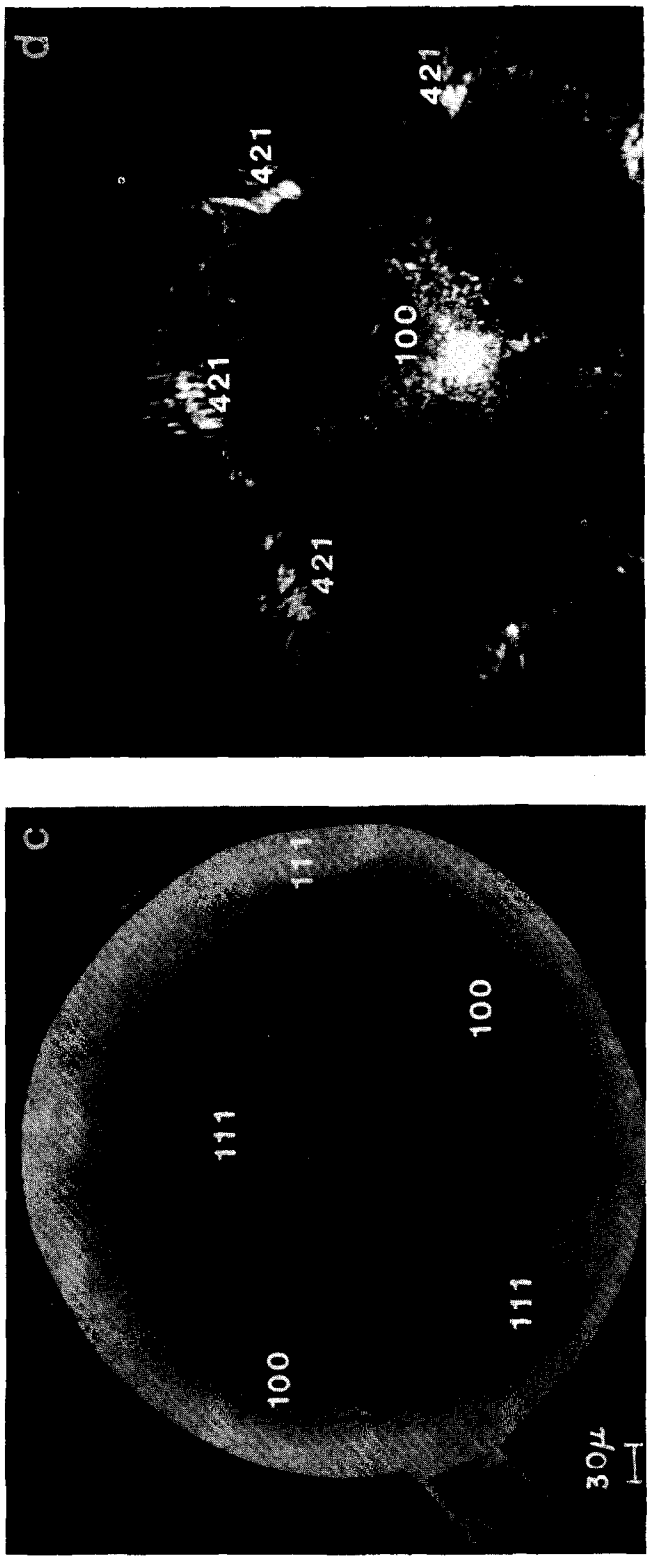

FIGURE 1c and d

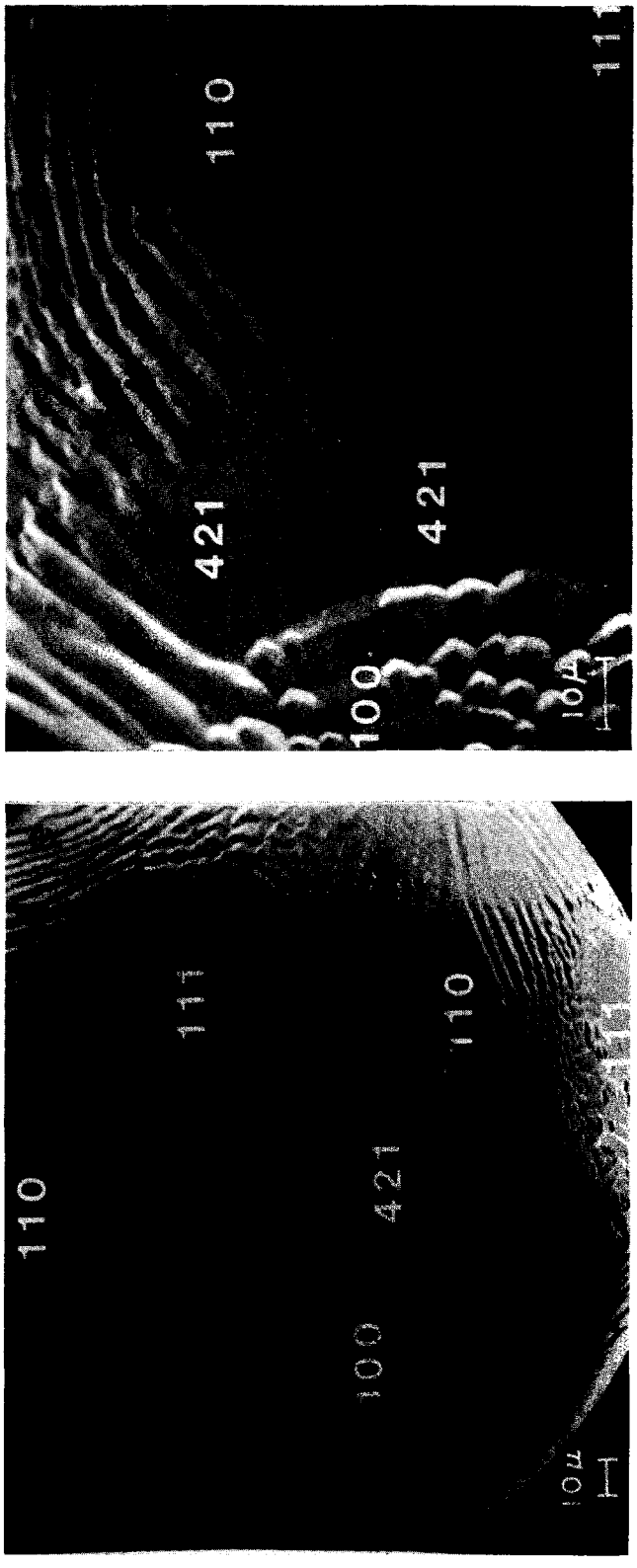

FIGURE 1e and f

angle which is the "unit cell" of possible orientations on a curved surface. A perfect single crystal sphere can therefore be decomposed into identical stereographic triangles, the structures of any one giving a complete characterization of the sphere. Further, the relative areas of various structures in the triangle are equal to the relative areas over the sphere, and the planar projection of this triangle (obtained from SEM micrographs) does not deviate from the true dimensions on the sphere by more than ~10% if the region being examined is near normal incidence. Etching structures were determined throughout the triangle by measuring relative distances from several micrographs at particular reaction conditions.

Miller indices of planes which we shall refer to are shown in Fig. 1a. We shall also describe families of planes or orientations along particular symmetry directions. In Fig. 1a we denote four of these as $(1XX)$, $(11X)$, $(21X)$, and $(1X0)$ with X a variable between 0 and 1. When normalized, these give the Miller indices of planes along these directions; for example, along $(21X)$, $X = 0.5$ corresponds to the (421) plane and $X = 0.25$ corresponds to the (841) plane. In micrographs we denote families of planes with Miller indices in decreasing magnitude without brackets rather than the more usual notation $[X, Y, Z]$.

While the (111), (100), and (110) planes can be identified from symmetry alone, orientations of other regions in the stereographic triangle can only be specified to within a few degrees from SEM micrographs, and variation between triangles or slight curvature are difficult to detect. Therefore, we used reflectance of a collimated laser beam to determine angles and variations of angles more accurately. Figure 1d shows a photograph of reflectance images projected on a flat screen. The incident light beam was nearly normal to the (100) (near bottom) and, since the angle between (100) and the eight bright spots around it was ~59°, these planes must be at one-half of this angle from (100) which fixes them along $(21X)$. The angle between the bright regions shows that they are close to {421}.

NH_3 Oxidation

We have examined NH_3 oxidation on Pt more extensively than other reactions, and in this section we consider dependences of morphology on gas composition, surface temperature, flow rate, and time. However, even for this system we regard our results as only qualitative indications of morphological changes. NH_3 reacts with O_2 to form NO or N_2 and H_2O through the reactions (*9*)

$$4NH_3 + 5O_2 \rightarrow 4NO + 6H_2O, \quad (1)$$

and

$$4NH_3 + 3O_2 \rightarrow 2N_2 + 6H_2O. \quad (2)$$

With air and NH_3 as reactants the stoichiometric compositions are 14 and 21% NH_3, respectively. Thus for less than 14% NH_3 the reaction occurs in excess O_2, and for higher compositions it occurs in excess NH_3. The industrial process is carried out in 10% NH_3 in which the conversion to NO is ~95% at 900C (*10*).

Initial structures in excess O_2. Figures 1e, f and 2 show micrographs of Pt for 10% NH_3 in air. Figures 1e through 2d are after 5 hr at 1100 K for flow velocities of ~5 cm sec^{-1}. These show "mild" faceting characteristic of the first stages of catalytic etching. We examined approximately 100 spheres under comparable condititions, and all without exception had morphologies nearly identical to those shown.

The {111} planes remain flat and have roughly the same size as on the unreacted sphere. The {100} planes are small, and rather large diamond shaped {110} planes form. The only other unfaceted plane is the {421} which is evident as a large region near the center of the stereographic triangle.

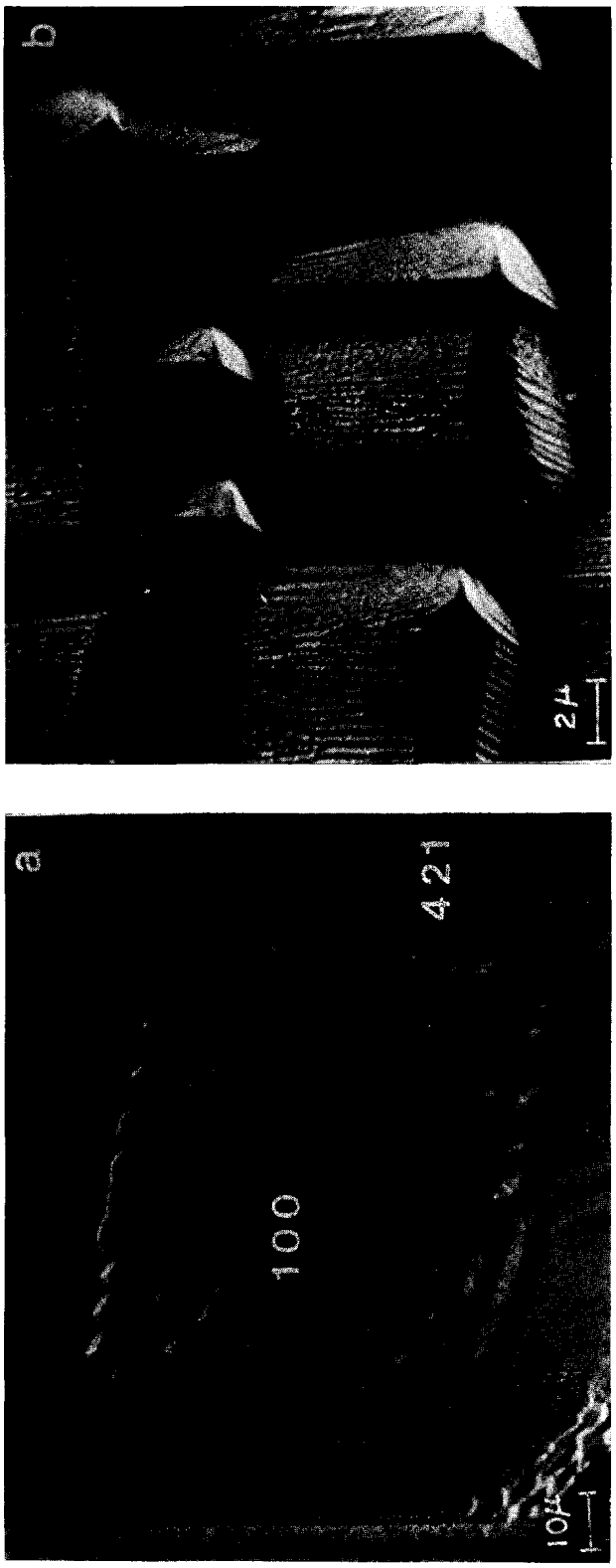

FIG. 2a–d. Micrographs of the {100} and {110} regions of the sphere shown in Fig. 1e. (a) {100} region; (b) detail near {100}; (c) {110} region; (d) detail near {110}; (e) micrograph of a 0.015 cm diameter sphere used in oxidation of 10% NH_3 in air after 5 hr. The {211} planes are indicated. (f) A Pt sphere used in 10% NH_3 oxidation after 100 hr of reaction.

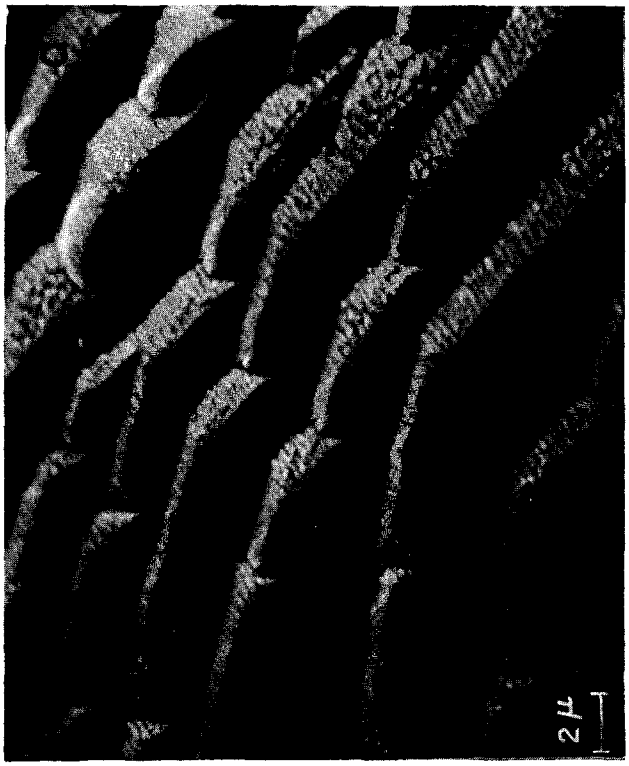

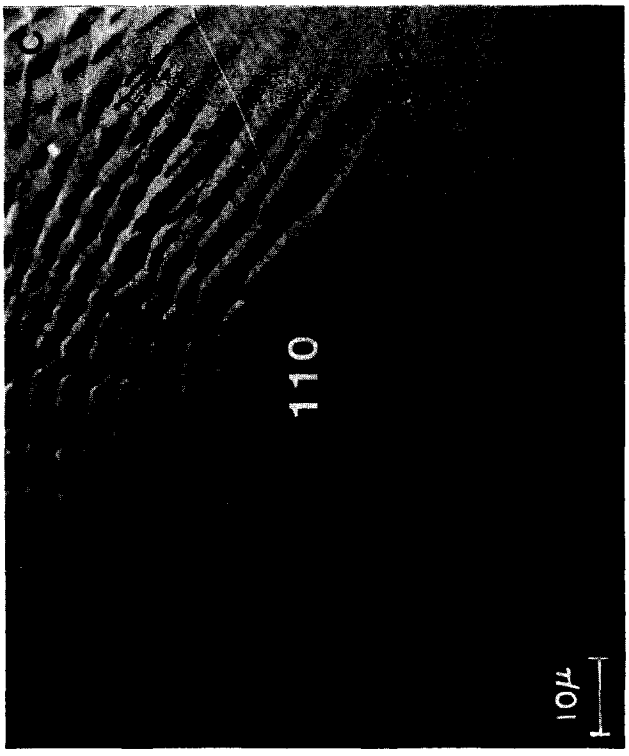

FIGURE 2c and d

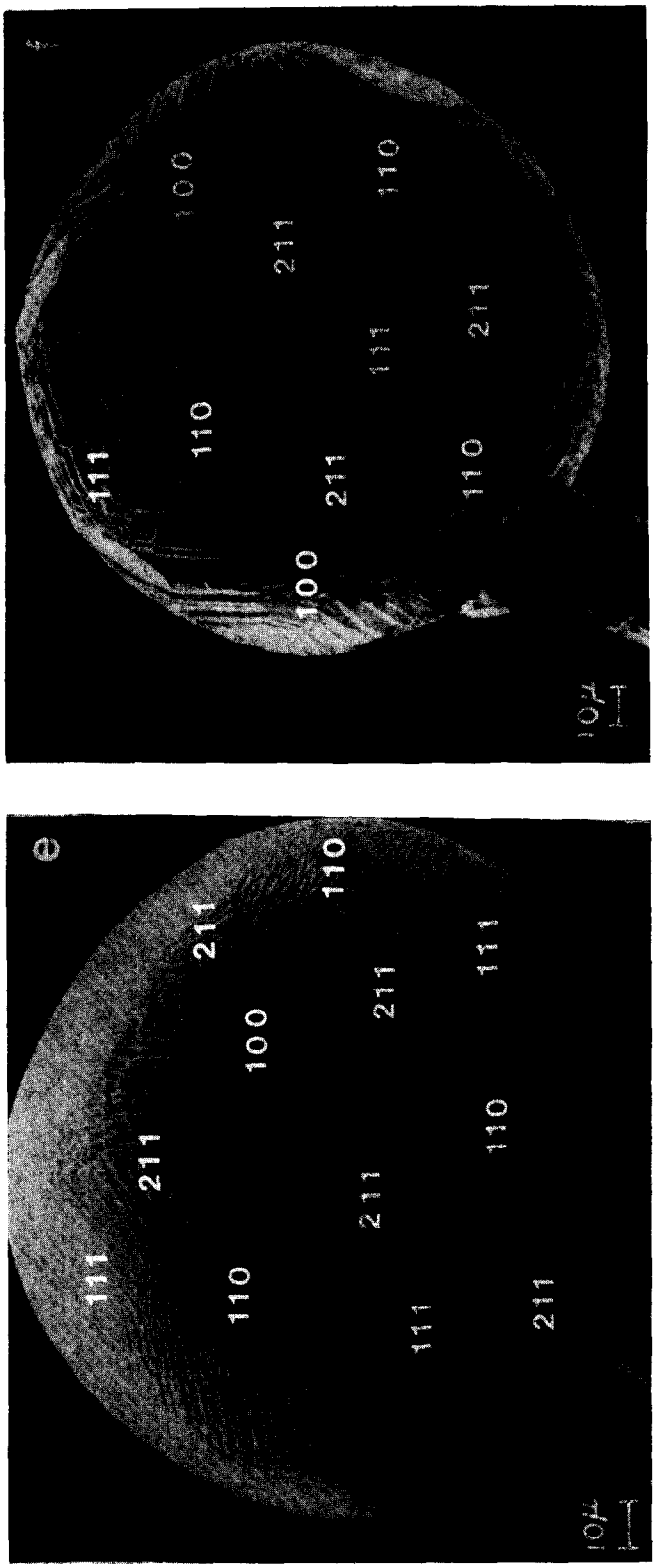

FIGURE 2e and f

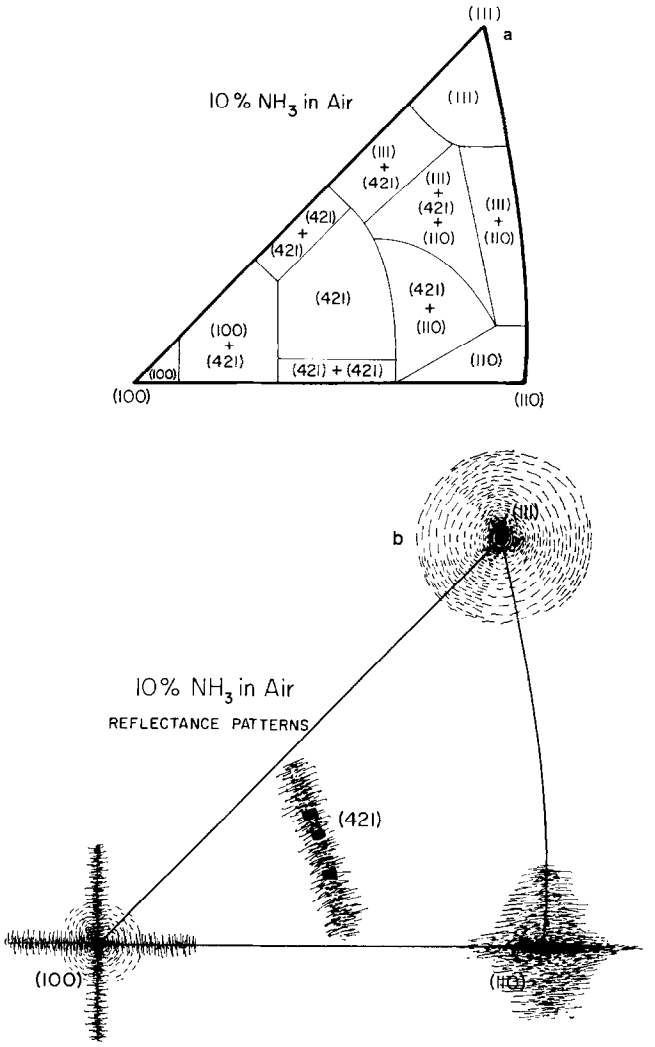

FIG. 3. Stereographic triangles constructed from several spheres used in 10% NH_3 oxidation after 5 hr at 1100 K. Major planes observed in various regions are indicated in (a) as determined from SEM micrographs such as in Fig. 1e. Relative areas of planes formed are indicated in (b) as determined from reflectance patterns such as shown in Fig. 1d.

All other regions are faceted into these planes. Figure 1e shows the planes found in various regions of the stereographic triangle. All major facets under these conditions are ~2–3 μm across. Most of these facets also exhibit smaller secondary facets which are typically 1000–3000 Å across, and some of these extend down in size to the resolution of the SEM.

Figure 3a indicates regions of flat planes and facet patterns over the stereographic triangle. As indicated, the {111}, {100}, {110}, and {421} planes are flat, while the rest of the triangle consists of regions of facets exposing predominantly one, two, or three of these four planes.

Figure 3b shows laser reflectance patterns from surfaces of this type. The bright spots at (100) and (111) subtend angles of ~1.5° which show that these planes are flat to within this angle. There is a broader region of reflecting planes (in facets) along

(21X) but this region is very sharp perpendicular to this zone. The dominant plane is near (421) with some planes extending between (843) and (841). No planes at (210) or (211) are observed on these spheres.

The range of planes observed is due to variations between planes in faceted regions. This is also evident from weak diffuse regions of spots around the much brighter (100) spots shown in Fig. 1d. Each weak spot evidently originates from a plane near (100) in facets. These facet planes are nearly uniform around (111) but form a cross [in the (1X0) direction] around (100) extending to the (410). Figure 3b shows laser reflectance patterns constructed on the stereographic triangle from several observations of spheres at different angles of incidence following NH_3 oxidation in 10% NH_3 in air. The cross around (100), the band along (21X) and the distribution of planes around (111) are indicated in Fig. 3b.

Relative areas of all four planes were estimated from the facet patterns of Fig. 1e by determining the areas of each region and associating with a particular plane all of the plane itself and one-half or one-third of those regions on which that plane was one of two or three facet planes, respectively. Fractional areas for NH_3 oxidation under these conditions are shown in Table 1.

Also shown in Table 1 are fractional areas for NH_3 oxidation under other conditions as indicated. We see that for an NH_3 air mixture with ~5% NH_3, the {111}, {100}, and {110} regions are flat, while all other orientations facet into these three planes (photograph not shown). The very small (0.008 cm diameter) sphere shown in Fig. 4a exhibits extensive faceting. In 5% NH_3 small (~1 μm) crystallites are observed to grow from facet ridges.

High flow rates. Figure 6a and b show a Pt sphere after reaction for 2 hr in 10% NH_3 in air with a high flow velocity of ~35 cm sec^{-1}. During the reaction the spheres were heated resistively to ~1100 K because adiabatic temperatures were somewhat lower than at lower flow rates. The {110} plane and the (1X0) zone have broken entirely into {100} and {111} planes. The {100} plane appears to comprise more of the total surface than the {111}, and for longer times the {111} may actually disappear entirely.

Long time experiments. Figure 2f shows a Pt sphere after reaction in 10% NH_3 in air for 100 hr and low flow rates. Extensively etched structures are observed with facet size generally increasing and its distribution expanding to 2–6 μm. The {111}, {100}, {110}, {210}, and {211} planes are observed.

Small spheres. Small spheres always exhibited more rapid and extensive etching than larger ones for this and all other reactions. As discussed below, this is expected from boundary layer considerations. As shown in Fig. 2e on a 0.015 cm diameter sphere the {211} plane is now observed in 10% NH_3 as contrasted with the larger sphere of Fig. 1e where the {421} dominated.

Initial structures in excess NH_3. Figure 4b and c show Pt spheres used in NH_3 oxidation with 20 and 50% NH_3, respectively for 5 hr at 1200 K for flow velocities of ~10 cm sec^{-1}. As in excess O_2, the {111}, {100}, and {110} planes are stable. In 20% NH_3 the {421} plane is still observed but now so also is the {210}. In 50% NH_3, however, the {421} plane is not observed, while the {210} and {211} planes appear. In Fig. 5a patterns formed are indicated on the stereographic triangle from SEM micrographs, and Fig. 5b shows planes formed as determined from laser reflectance patterns for a 20% NH_3 in air mixtures.

High temperature. Figure 4d shows a sphere heated resistively to 1500 K in 20% NH_3 for 5 hr. On this surface the region within ~20° of {100} is smooth and curved,

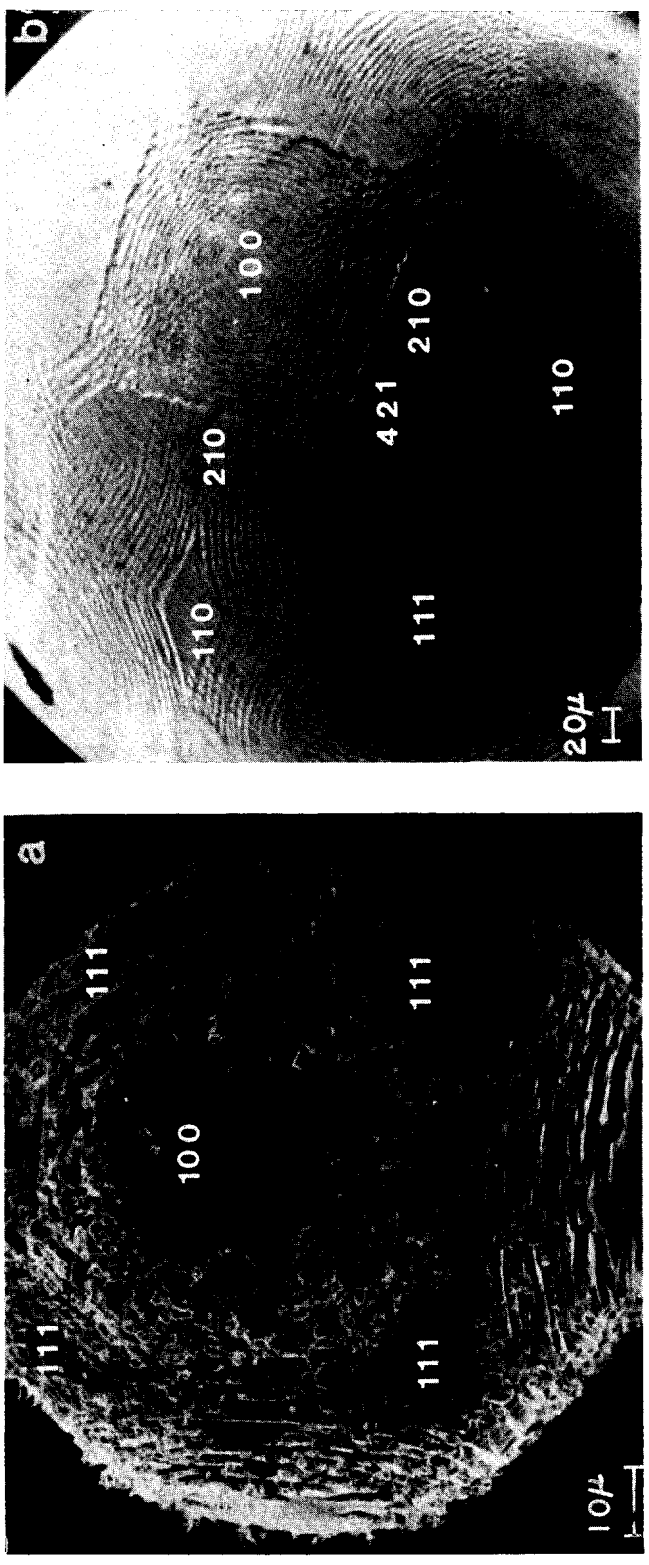

FIG. 4a. Micrograph of a 0.01 cm diameter Pt sphere exposed to 5% NH_3 in air for 3 hr at 1050 K. (b) and (c) Spheres used in excess NH_3 at 1200 K for 5 hr. In (b), for 20% NH_3 in air, the {421} and {210} planes are indicated. For 50% NH_3 in air, as in (c), no {421} planes are observed. The {211} and {210} planes appear in addition to {111}, {100} and {110}. (d) Micrograph of a sphere heated to 1500 K in 20% NH_3 for 5 hr. Curved surfaces are evident, and the {111} and {100} planes are the only stable flat planes. (e) and (f) A sphere used in 10% NH_3 in air for 5 hr at 1600 K is shown. Randomly spaced pits of ~5 μm in diameter cover the surface.

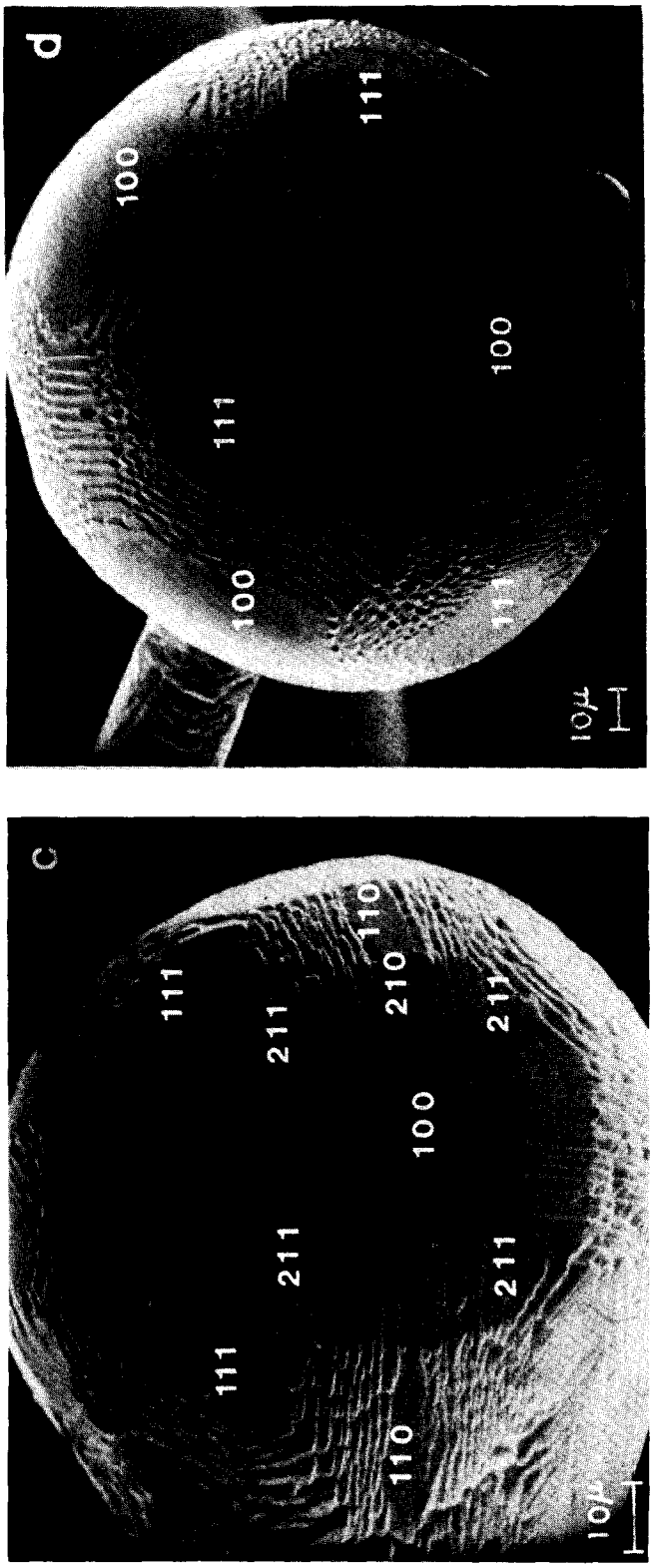

FIGURE 4c and d

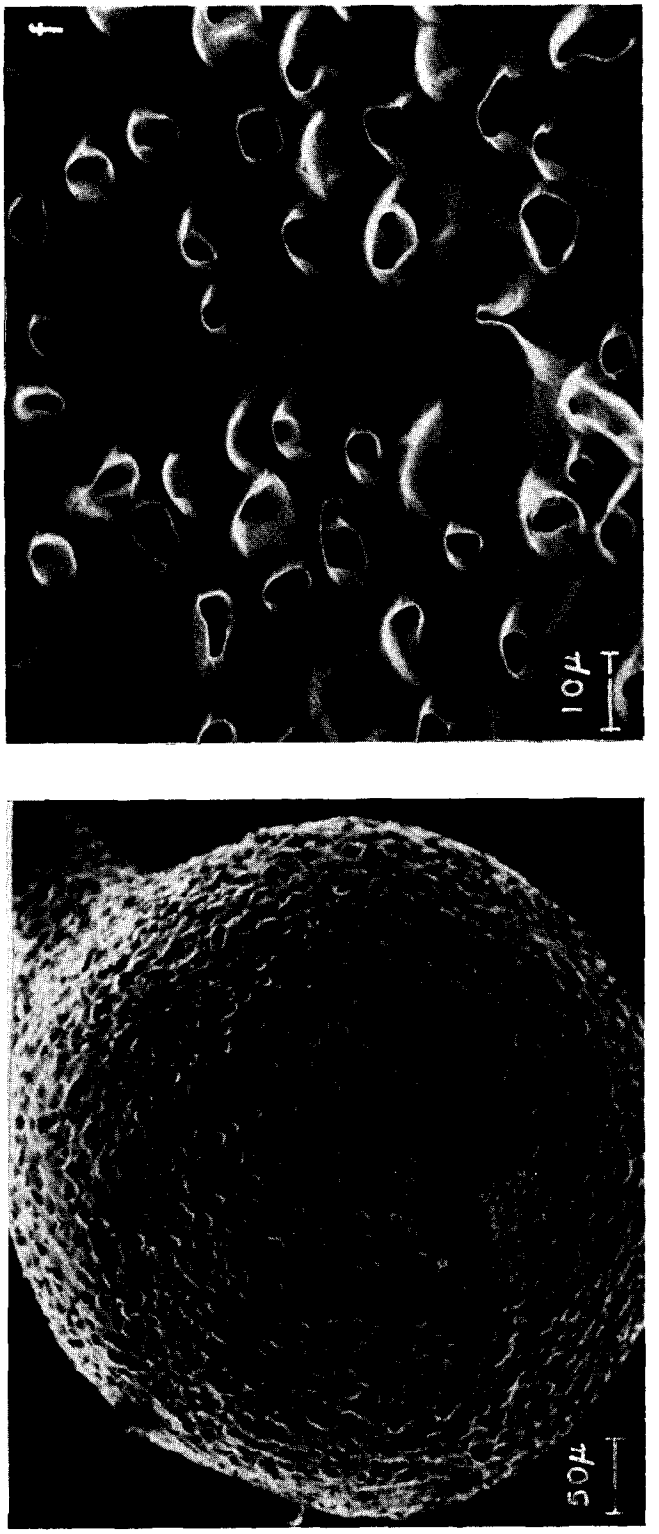

FIGURE 4e and f

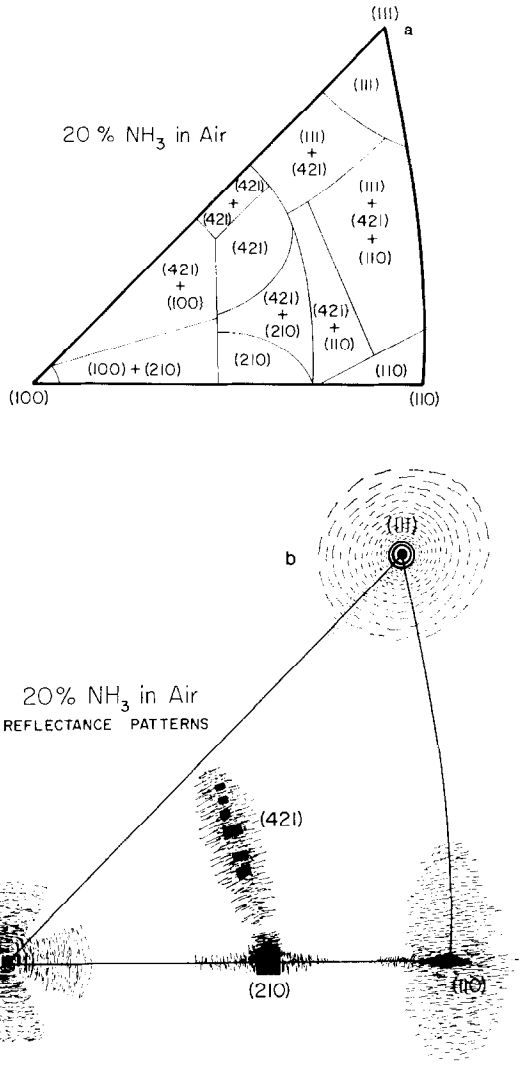

FIG. 5. Stereographic triangles constructed from several spheres used in 20% NH_3 oxidation after 5 hr at 1200 K. Major planes observed in various regions are indicated in (a) as determined from SEM micrographs such as Fig. 4b. Relative areas of planes formed are indicated in (b) as determined from reflectance patterns such as shown in Fig. 1d.

the region near {111} exhibits facets of {111} and {100}, and the {110} region has broken into exclusively {100} facets.

Heating resistively to temperatures further above the adiabatic temperature results in pitting of the metal surfaces for all mixture compositions. Figure 4e and f show a Pt sphere after reaction in 10% NH_3 in air for 5 hr at 1600 K (adiabatic $T \sim 1100$ K). The surface shows randomly spaced irregular pits of ~ 5 μm in diameter, and no crystallographic variations are noted. Similar results were obtained for spheres heated in excess NH_3 mixtures at $T > 1600$ K.

Pd, Rh, and alloys. Figure 7 shows spheres used in NH_3 oxidation in 10% NH_3 for Pd (1100 K), Rh (1300 K), and a Pt–30% Rh alloy (1250 K). The alloy was formed from high purity wire, but the

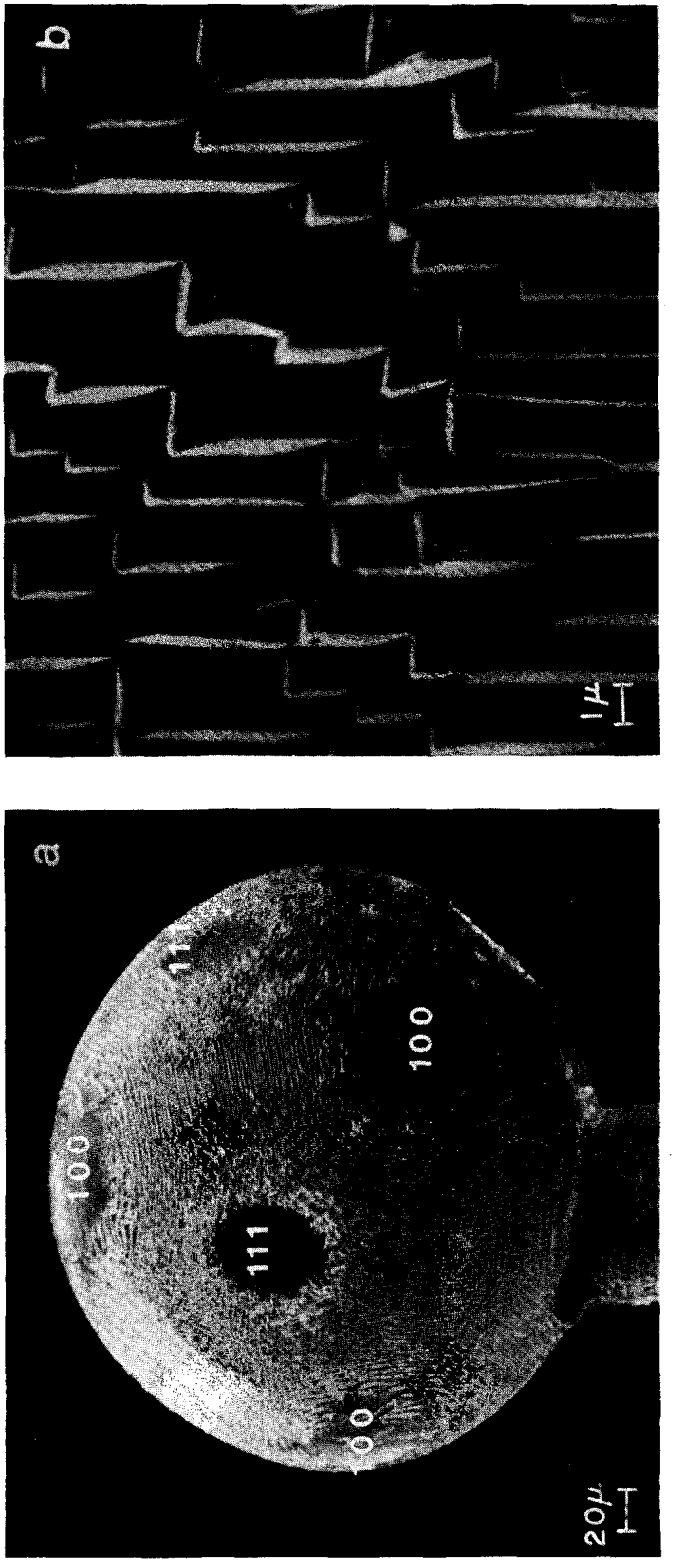

FIG. 6a and b. Micrographs of spheres used in 10% NH_3 oxidation at a flow rate of 35 cm sec^{-1} after 2 hr at 1100 K. The entire surface consists of {100} and {111} planes. (c) Platinum sphere used in NH_3 decomposition at 1250 K for 2 hr. (d) After 22 hr the {111} and {421} regions appear flat, while the {100} is flat only near the pole. (e) and (f) Sphere heated to 1500 K in NH_3 for 5 hr. Curved surfaces and pits of an average size of ~2 μm are observed.

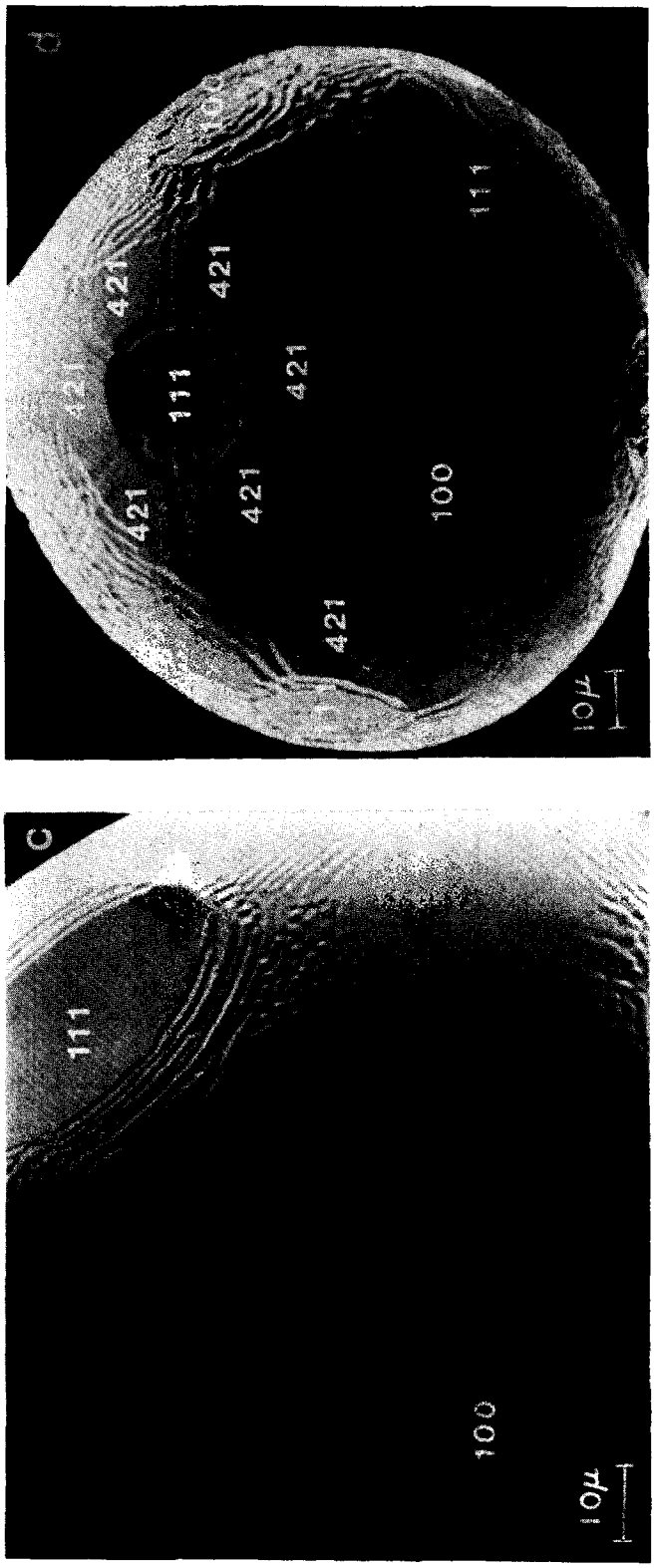

FIGURE 6c and d

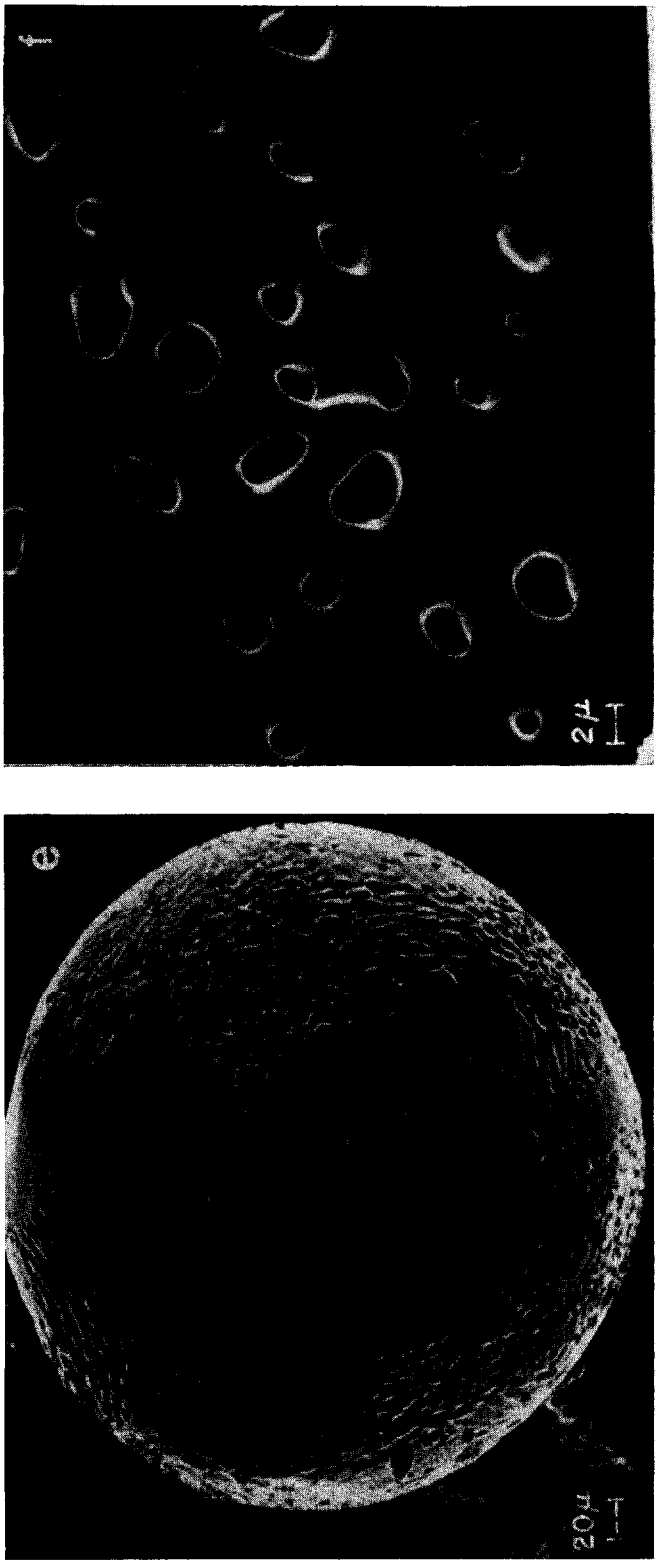

FIGURE 6e and f

composition should, of course, vary slightly over the sphere because solidification does not occur over the sphere instantaneously. The temperatures quoted are adiabatic ones, the small difference presumably being due to difference in reaction rates.

Palladium exhibits only pits (see Fig. 7a and b). These range in size from 2 μm down to the $\sim$200 Å resolution of the SEM. In unpublished work we have observed that pit formation occurs within 1 min even at 800 K on polycrystalline Pd wires.

Figure 7c and d show a Rh sphere. Two grain boundaries are visible, but the {111}, {100}, and {110} planes are easily identified from symmetry. The {111} is nearly circular and ledges near {111} apparently consist of several planes. Pyramidal structures are evident over all the surface but these structures have higher densities on {100} and {111} planes. Pits cover most of the surface but they are observed to concentrate on the ridges formed at the grain boundaries and at the stepped surfaces around the planes (e.g., Fig. 7d). More experiments with Rh single crystals are in progress to find the mixture compositions and temperatures for which the surface facets without pitting and thus identify the crystallographic specificity of the reaction rate on these surfaces.

On the Pt–30% Rh alloy, shown in Fig. 7e, there were several grain boundaries on all spheres, but crystals could be easily identified from symmetry. As on Pt, the {110} region exists as a diamond shaped plane but the {100} is large and curved, and the {111} appears to be much smaller than on pure Pt. No enhanced pitting or crystallite formation are observed on this alloy.

NH_3 Decomposition

This is an endothermic reaction, and therefore the spheres were heated resistively. Faceting is much slower than with oxidation reactions, presumably because the absence of volatile PtO_2 eliminates vapor oxide transport.

Figure 6c shows a sphere after 2 hr at 1250 K with an NH_3 flow velocity of 5 cm sec^{-1}. Faceting has begun around the {111} and {100} planes, but large regions around {110} and {211} remain smooth and curved. The parallel facets in the "X" around {100} consist of planes near {421}, and parallel facets around {111} consist of {111} plus either {211} or {421}.

Figure 6d shows a sphere which had been heated for 22 hr at 1250 K with an NH_3 flow velocity of 2 cm sec^{-1}. Etching patterns are similar to those after 2 hr except that the regions near {110} and {211} are now faceted and the {421} regions appear as flat planes. The {100} planes have shrunk and almost disappeared. There appears to be a flat plane along (11X) which may be a {331}, and the {110} appears to have faceted into these planes.

At higher temperatures in pure NH_3 the morphology exhibits distinct differences from that just noted for $T < 1250$ K. At 1500 K pits form as shown in Fig. 6e and f. Metal is deposited at the pit mouth and the pit walls are generally curved. Pit densities do not appear to be strongly dependent on crystallographic orientation. The average pit size is $\sim$2 μm.

Figure 9a shows facet patterns on stereographic triangles for the low temperature conditions, and Table 1 indicates the fractions of various planes on the surface.

Propane Oxidation

This is a very fast exothermic reaction, and the reactant composition had to be far from the stoichiometric ratio (3.8% C_3H_8 in air for reaction to CO_2) to avoid excessively high temperatures and homogeneous reaction. In excess C_3H_8 the surface became uniformly covered with 0.3 μm diameter spheres, presumably carbon black, as shown in Fig. 7f. Under some conditions the reaction would quench after a short time,

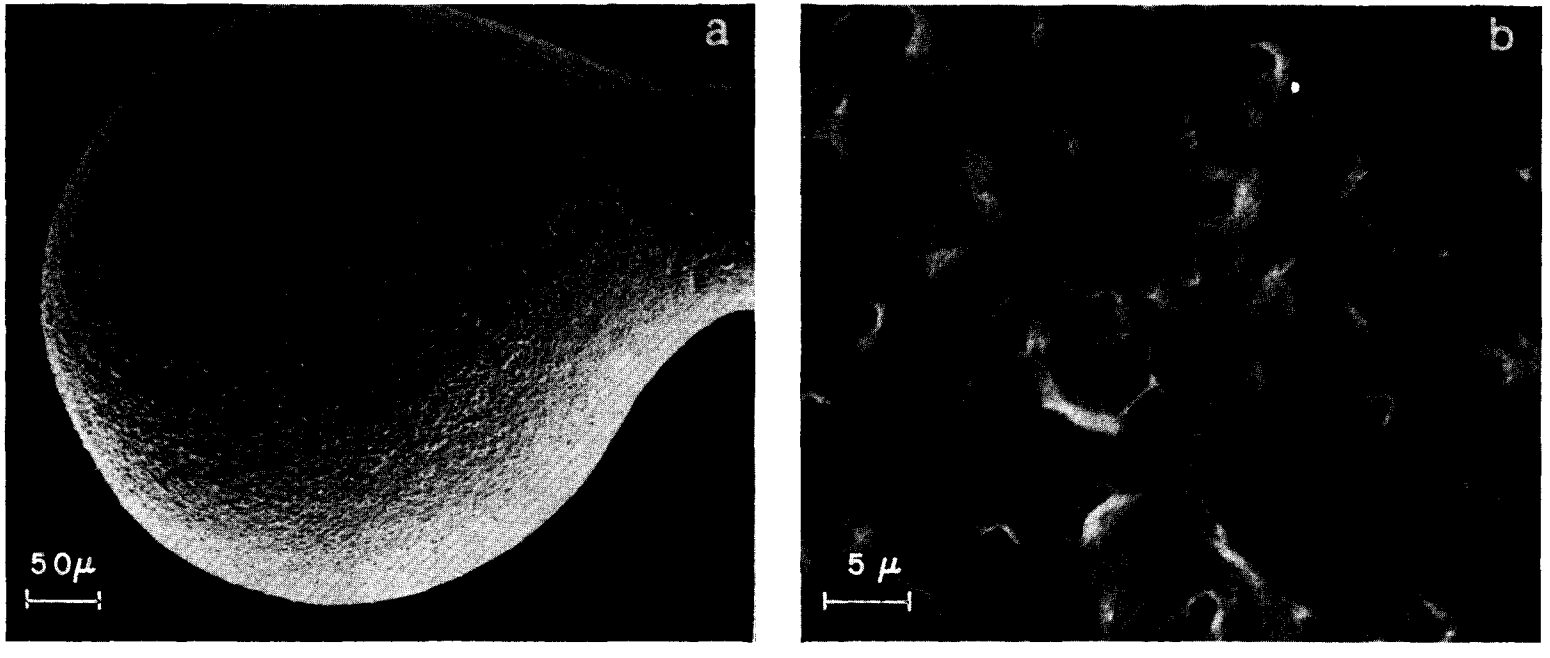

FIG. 7a and b. A 0.04 cm diameter Pd sphere is shown after it was used for 1 hr in 10% NH_3 in air at 1100 K. Only pits are exhibited on the Pd surface. (c) and (d) A 0.05 cm diameter Rh sphere after 5 hr in 10% NH_3 oxidation at 1300 K. Pits cover most of the surface. For regions near {111} pits are concentrated on the stepped surfaces. (e) Micrograph of an alloy sphere (Pt–30% Rh) used in 10% NH_3 oxidation at 1250 K. Grain boundaries and stable {100}, {111} and {110} planes are observed. (f) Carbon spheres deposited on platinum used in 14% C_3H_8 in air mixtures at 1000 K.

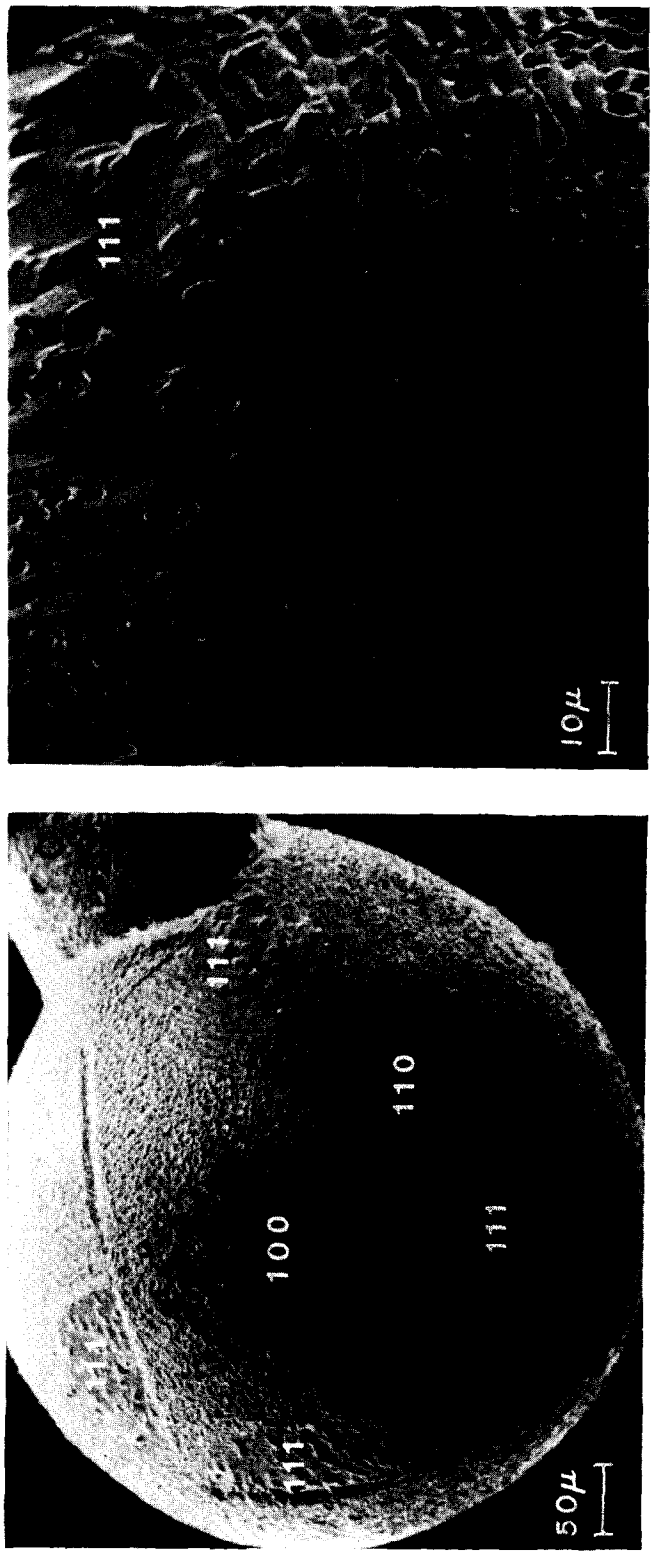

FIGURE 7c and d

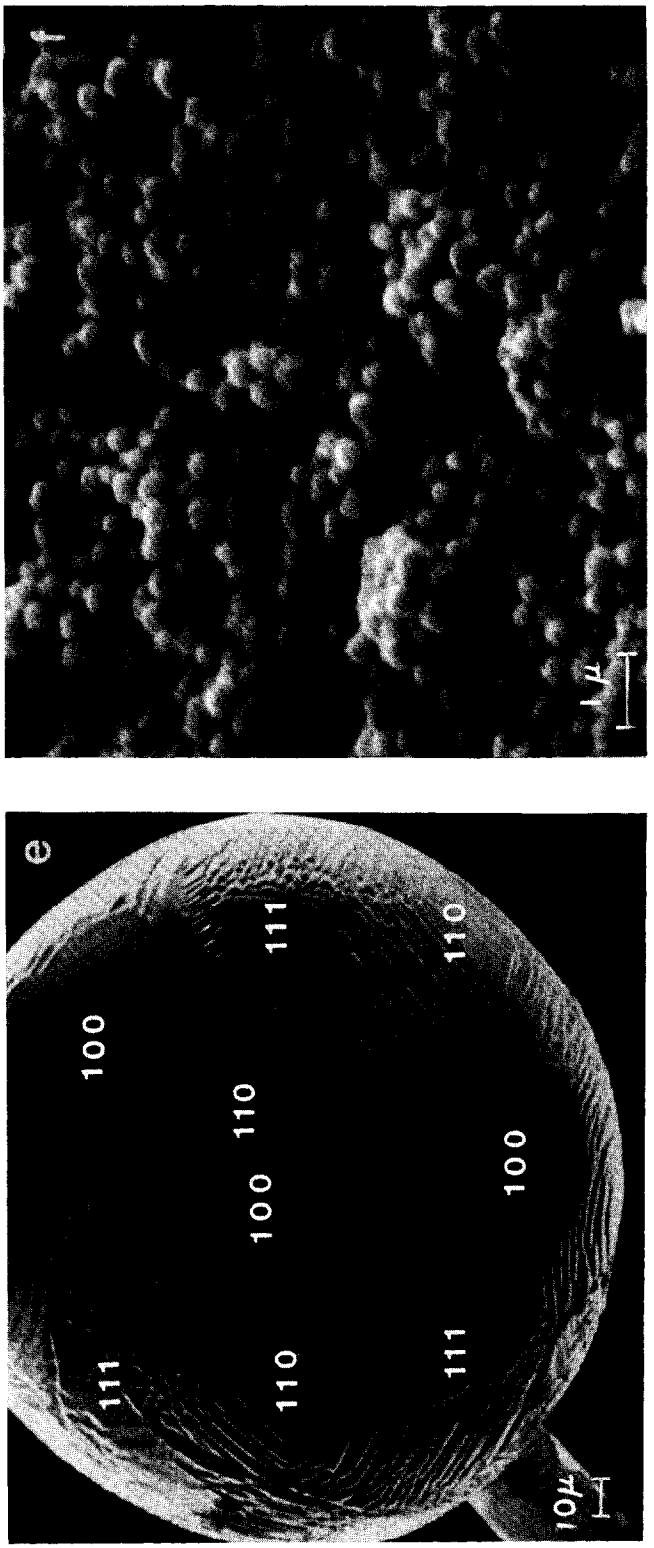

FIGURE 7e and f

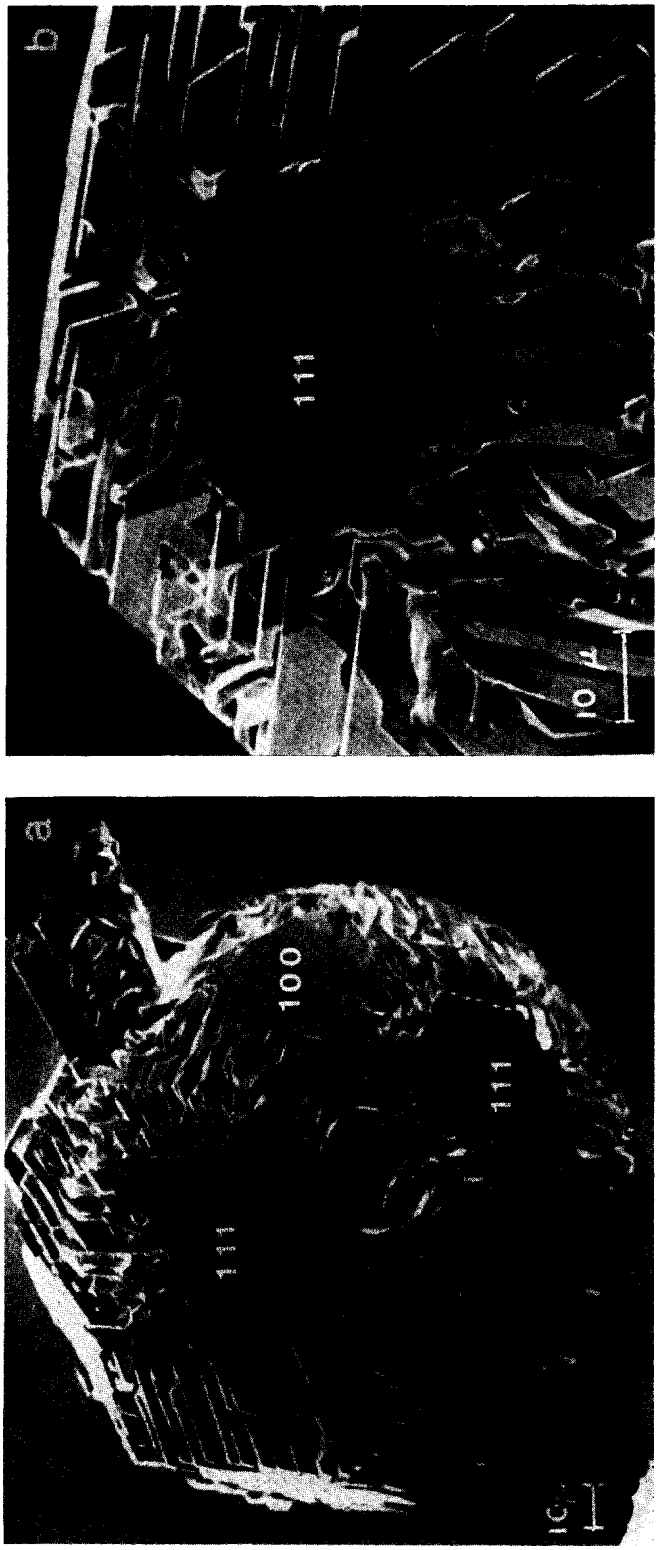

FIG. 8a and b. Heavily faceted spheres used in ~2% C_3H_8 oxidation exhibit only {100} and {111} planes with extensive undercutting. (c) and (d) Micrographs of a 0.02 diameter sphere used in 50% CO oxidation at 1150 K for 2 hr. The surface consists of {111}, {100} and {310} planes around which faceting has advanced. (e) and (f) A platinum sphere exposed to 10% CO at 1250 K for 2 hr. Irregular structures have preferentially built up on low index planes. On {111} pits are observed.

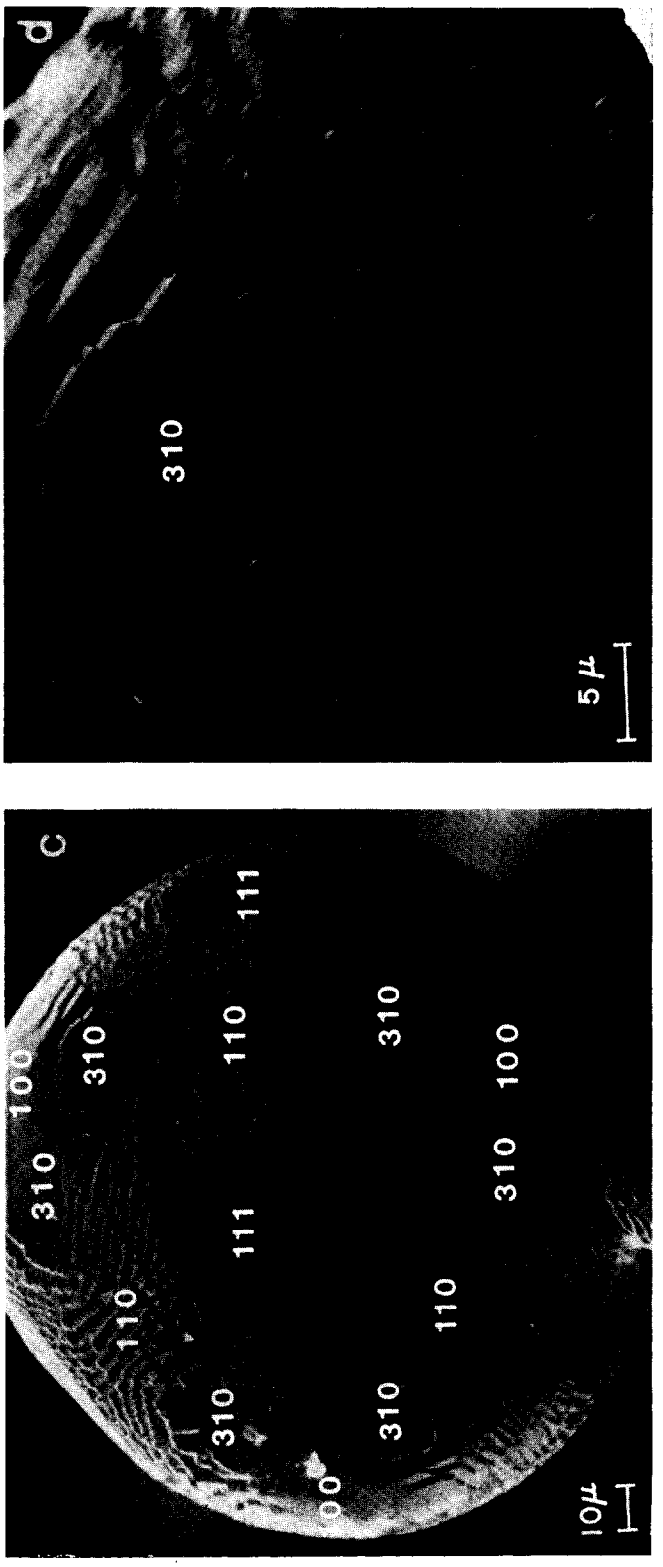

FIGURE 8c and d

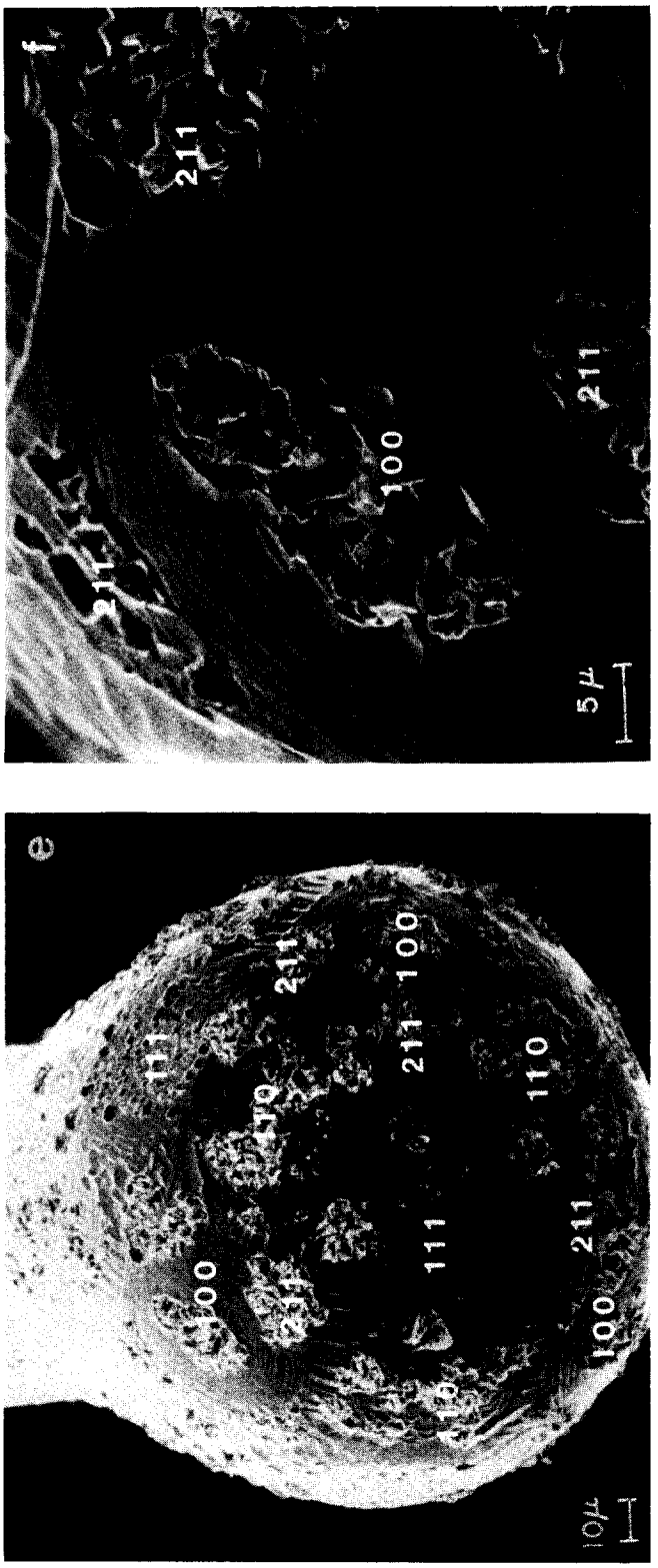

FIGURE 8e and f

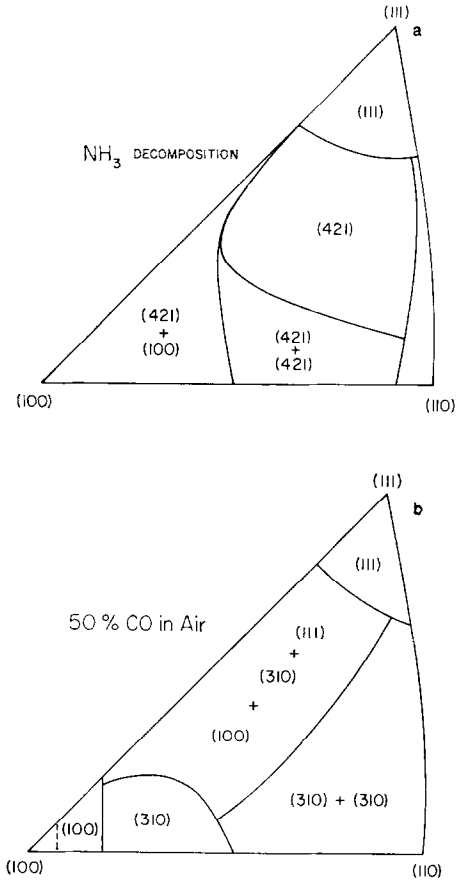

FIG. 9. Stereographic triangles constructed from spheres used in NH_3 decomposition (a) and in 50% CO oxidation (b). Planes are indicated from SEM micrographs such as shown in Figs. 6d and 8c. respectively.

probably because of carbon formation. All reactions were therefore run at 2–3% C_3H_8 in air.

Figure 8a and b show spheres used in C_3H_8 oxidation at ~1100 K for 2 hours. All regions except {100} and {111} have become faceted, and all facets are sufficiently flat and regular that it is evident that predominantly {100} and {111} planes exist on this surface. We also used laser reflectance from those surfaces to show that {100} and {111} planes comprised the only major planes. The {210} planes were observed for short times in this reaction (not shown), but they disappeared for longer times.

The micrographs also reveal that extensive undercutting occurs on these surfaces, i.e., there are channels dug into the surface with parallel facing planes. These occur regularly at the bottom of facet grooves in most crystallographic orientations.

CO Oxidation

Platinum single crystal spheres were exposed to CO and air mixtures at compositions above and below the stoichiometric ratio (30% CO in air). Figure 8c and d show spheres exposed to 40–50% CO in air at 1150 K for 2 hr. The {111}, {100}, and {310} regions are flat, while the {110} region breaks up entirely into {310} facets.

Figure 8e and f show a sphere exposed to 10% CO in air for 2 hr at temperature 1250 K at a flow velocity of ~4 cm sec^{-1}. Irregular structures are observed on the {100} and {110} planes and pits are the dominant structures on {111}. The regions surrounding these planes are faceted. On smaller spheres or for longer times the entire surface was broken into these irregular built-up structures. Investigations are currently in progress to identify these structures. Figure 9b shows facet patterns on stereographic triangles for Pt spheres exposed to 40–50% CO in air mixtures. These surfaces exhibit only the normal flat plane and facet patterns observed with other reactions. Table 1 indicates the fractions of various planes on these surfaces.

DISCUSSION

As we have noted previously (*3*), the surface catalytic reactions can set up very large concentration and temperature gradients which would not exist in the absence of reaction. Consequently, while these processes appear to be similar in many ways to thermal etching which is observed when metals are heated for long times in vacuum, O_2, or inert atmospheres (*1*, *2*), the reaction

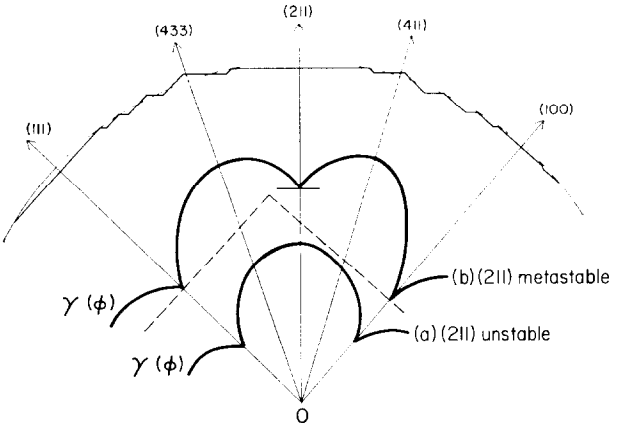

FIG. 10. Diagram illustrating stable, metastable, and unstable orientations from surface free energy γ vs orientation ϕ. The zone between {111} and {100} is chosen as an example.

can provide qualitatively different mechanisms of etching than in thermal etching. However, in spite of the considerable simplifications in thermal etching situations compared to catalytic etching, mechanisms of thermal etching are only qualitatively understood at best, and few predictions of etching have been attempted.

In the next section we shall consider the predictions of surface free energy on the stability and metastability of these surfaces. In following sections, we shall consider metal transport through surface and volatile oxide diffusion and also effects of the boundary layer on the etching process.

Surface Energy Considerations

Many of the structures observed here appear to be explainable as a consequence of minimum surface free energy. The equilibrium shapes of crystals have been discussed in detail by Herring and others (*11–13*). In equilibrium a surface with planes of area A_i and specific surface free energy γ_i will correspond to

$$\Sigma A_i \gamma_i, \qquad (3)$$

being a minimum subject to constraints at boundaries, from mass conservation, etc. In practice the temperature, time, and gas environment will determine the constraints and control the approach to the equilibrium shape. A polar plot of γ versus orientation ϕ (Wulff plot) should exhibit cusps at several minimum energy planes (Fig. 10), and Herring (*11*) showed that the equilibrium shape of a single crystal can be found by constructing tangent planes normal to a radius from the origin through these cusps. If planes can be constructed which lie wholly inside $\gamma(\phi)$, the crystal will be a polyhedron of these planes, and, if they intersect $\gamma(\phi)$ in some regions, the crystal will have both flat planes and curved regions. Freshly formed spheres, Fig. 1c, presumably exhibit the equilibrium shape frozen in near the melting point which has just sufficient variation in $\gamma(\phi)$ to form {111} and {100} planes.

Gas adsorption should in general lower γ's and alter crystallographic anisotropies (*14*), and this fact may explain the different stable planes observed on Pt catalysts. On the clean surface most models (*15*) predict $\gamma_{111} < \gamma_{100} < \gamma_{110} \leq \gamma_{211} \leq \gamma_{210}$ and this is roughly the order of stability we observe. However, large anisotropies may be created by gas adsorption if there are large heat of adsorption anisotropies, and the identification of stable planes on

catalysts may be quite unpredictable from clean surface structures.

Rates of facet formation. These considerations also predict metastability versus instability of various orientations (*16*) and suggest the relative rates of facet formation. A plane will be thermodynamically unstable if $\gamma(\phi)$ at this orientation lies outside the polyhedron of tangent planes, and this plane will facet into these planes. As indicated in Fig. 10a, with $\gamma(\phi)$ as sketched, the (211) plane would be unstable and this orientation would form (111) and (100) facets. However, this plane would be metastable if $\gamma(\phi)$ were as shown in Fig. 10b because of a cusp at this orientation. This plane would only break up into facets if nucleated by local surface roughness or at orientations near the maximum in γ (drawn as (433) and (411) planes in this example). Therefore, an orientation such as (411) on a smoothly curved surface may first break up into (211) and (100) planes, and then the (211) facets may later break into smaller (100) and (111) facets.

Relative rates of facet formation should be correlated with features of $\gamma(\phi)$. Faceting will occur most rapidly near cusps where the gradient in γ is largest. The first facets should therefore be observed around stable or metastable planes.

Regions near the maximum in γ are stable towards small orientation variations because, if γ is almost constant, the total surface area should be a minimum according to Eq. (3). These regions will therefore facet at a later stage on an initially smooth surface and faceting should originate at edges. The last regions to facet into their equilibrium structures should be the metastable planes, and these may also exhibit breakup nucleated from the edges where unstable orientations first form.

Facet size. Mullins (*16*) solved the diffusion equation for formation of parallel facets for transport by surface diffusion and gas diffusion. He showed that with fixed parameters (a specified orientation) the facet width l should increase with time as

$$l \sim t^{\frac{1}{4}} \text{ for surface diffusion,}$$

while for gas diffusion (transport of the metal vapor through the ambient gas) or for volume diffusion

$$l \sim t^{\frac{1}{3}}.$$

The width of facets for a given time should, by the previous argument, also depend on the local gradient in γ. Near cusps, facets should be small and near maxima facets should be larger. Transport properties may vary significantly with orientation, and this could also affect facet formation rate and size. Secondary facets (small facets on faces of larger ones) may result from either metastable planes which facet after the primary process is complete or from transport limitations (*1*, *16*).

Shapes and surface areas of crystals. The γ plot presumably predicts polyhedra for sufficiently small spheres (diameter comparable to facet size) in equilibrium with their surroundings, while for large spheres the total surface free energy can be minimized by forming hill and valley structures which follow the contours of the original sphere.

The increase in surface area of a sphere upon formation of facets much smaller than the diameter d can be calculated simply by computing the ratio of the area of the polyhedron containing the observed planes to the area of the sphere tangent to this polyhedron. This is easily visualized as the unfolding of the corrugated facets into a regular polyhedron. As an example when a spherical crystal facets into {100} planes the increase in area is $6d^2/4\pi(d/2)^2 = 1.91$. [Note, however, that if a spherical crystallite transforms into a cube, the area ratio is only $(6/\pi)^{\frac{1}{3}} = 1.24$ under the constant volume requirement.] Similarly, for regular polyhedra whose faces are tangent to the sphere, the area ratios are

1.28 for {111} and {100} planes, 1.31 for {100} and {110} planes, and 1.14 for {111} and {100} and {110} planes.

Transport Processes

Both surface diffusion and boundary layer diffusion of metal or volatile oxides are possible transport paths which may produce the metal migration observed here. It is easy to show from dimensional arguments that both mechanisms are feasible for most of our reaction conditions.

Volatile oxides. The vapor pressure of Pt is 6.7×10^{-9} Torr at 1570 K (*17*) and this is far too low to account for facet formation in the times of these experiments. However, Pt forms volatile oxides, mainly PtO_2, through the reaction

$$Pt(s) + O_2(g) \rightarrow PtO_2(g). \qquad (4)$$

For an O_2 pressure of 1 atm the equilibrium partial pressure of $PtO_2(g)$ is $\sim 2 \times 10^{-5}$ Torr at 1100 K (*18*).

We assume that the catalytic reaction varies considerably between two crystal planes which form stable facets such that the O_2 partial pressure (or more properly its chemical potential since the distance between facets is comparable to the gaseous mean free path) is low on the reactive plane and high on the unreactive one. The flux of metal, J_{Pt}, from one plane to another through volatile oxide is

$$J_{Pt} = -D_{PtO_2} \nabla C, \qquad (5)$$

and equilibrium in Eq. (4) could produce a PtO_2 partial pressure difference which approaches 2×10^{-6} Torr for 10% NH_3 in air at 1100 K. We now assume that ∇C parallel to the surface is approximately equal to $P_{PtO_2}/RT_s l$ for parallel facets of width l. In 1 hr a buildup of ~ 1 μm in facet height is observed which for parallel facets requires a metal flux, J_{Pt}, of 10^{15} atoms cm^{-2} sec^{-1} from an inactive to an active facet. The calculated value for the diffusion coefficient D_{PtO_2} is then ~ 2 cm^2 sec^{-1} which is in the range of values usually quoted for gases.

This dimensional argument shows that volatile oxide transport is feasible for reactions where O_2 is a reactant if crystallographic anisotropies in the catalytic reaction are sufficiently large. However, vapor transport cannot account for facet formation in NH_3 decomposition where no O_2 is present and it does not seem to be likely for oxidation reactions in large excesses of fuel because the O_2 (and consequently PtO_2) partial pressure should be small near the surface.

In some reactions such as C_3H_8 oxidation, with excess O_2, Fig. 8a, it appears that some regions are eroded away without a corresponding buildup on adjacent regions or planes. This phenomenon may arise from diffusion of PtO_2 through the boundary layer and away from the surface (*19*). The difference in metal evaporation rates between planes could arise either with equilibrium in Eq. (4) and a large difference in O_2 partial pressure or from different rates of the forward reaction in Eq. (4).

Surface diffusion. The surface self-diffusion coefficient of Pt is 7×10^{-8} cm^2 sec^{-1} at 1100 K (*20*) and there is evidence that it is much higher in the presence of gases (*21*). We assume that the catalytic reaction produces a large difference in surface mobility of Pt on the planes forming parallel facets. We write the flux equation as

$$J_{s,Pt} = -D_{s,Pt} \nabla n, \qquad (6)$$

where n is the surface density of the diffusing species. Taking ∇n as $n/l = 10^{15}/10^{-4} = 10^{19}$ atoms cm^{-3} and for an estimated surface flux of $\sim 10^{11}$ atoms cm^{-1} sec^{-1}, we obtain $D_{s,Pt} = 10^{-8}$ cm^2 sec^{-1}. This is slightly lower than the measured value for Pt self-diffusion at 1100 K, and we conclude from this estimation that surface diffusion is also a feasible Pt transport path in catalytic etching.

Boundary Layer Effects

At 1 atm the diffusive mass transfer rate to a 0.01 cm diameter sphere is $\sim 1 \times 10^{20}$ molecules cm^{-2} sec^{-1}, while extrapolations of low pressure rate measurements (*22*, *23*) predict rates much greater than this value. This indicates that all of these reactions are probably mass transfer limited. A possible exception is NH_3 decomposition which, because the rate is zeroth order at low temperatures, should have a reaction rate of $\sim 10^{20}$ molecules cm^{-2} sec^{-1} at 1500 K (*24*).

Therefore, the boundary layer controls concentrations and concentration gradients near the surface, and we shall show that this can explain the observed influences of flow velocity and sphere diameter on etching rates and morphologies. There are also large temperature gradients near the surface because the surfaces are between 800 and 1500 K while the flowing gas stream is at 300 K. However, for these qualitative considerations we shall ignore thermal boundary layer effects. Calculations indicate that there should be a negligible temperature gradient over the surface.

In steady state the catalytic reaction rate r_R for a first order reaction should be given by an expression

$$r_R = k_R P_{i\mathrm{S}} = k_M (P_i - P_{i\mathrm{S}}), \qquad (7)$$

where k_R is the reaction rate constant, k_M is the mass transfer coefficient, and $P_{i\mathrm{S}}$ and P_i are the surface and free partial pressures of reactant i. If mass transfer is important, $P_i \gg P_{i\mathrm{S}}$, and k_M must be determined to obtain the rate.

The mass transfer coefficient k_M is given by the expression

$$k_M = \frac{\mathrm{Nu}\,\mathfrak{D}_{AB}}{dRT_g}, \qquad (8)$$

where $\mathfrak{D}_{AB}$ is the binary diffusion coefficient, d the sphere diameter, and Nu the Nusselt number for mass transfer. For flow around a single sphere Nu for forced convection mass transfer should be approximately 2 for flow velocities less than ~ 10 cm/sec. For d = 0.01 to 0.1 cm, Eq. (7) predicts $k_M P_i = \sim 10^{20}$ to $\sim 10^{19}$ molecules cm^{-2} sec^{-1}. This justifies the assumption of mass transfer limitation because the reaction rates would be much larger than this for reactant partial pressures equal to their bulk values. This expression also predicts a rate inversely proportional to d which is consistent with the observed higher faceting rates on small spheres.

At a flow velocity of 35 cm sec^{-1} we observe different crystal planes and relative areas than for low flow velocities. For $v > 10$ cm sec^{-1} Nu becomes dependent on v, and with v = 35 cm sec^{-1} and d = 0.5 mm, we estimate Nu = 3.7. Thus, mass transfer correlations predict morphologies and rates independent of flow conditions but sensitive to flow conditions above this velocity. Our results are consistent with these estimations, but we have not varied flow velocity systematically, and flow profiles are probably not those of isolated spheres in these experiments.

SUMMARY

These results show that the surface morphologies produced by catalytic reactions are extremely sensitive to all variables thus far considered, and it is almost certain that other important variables will be discovered. We emphasize that the present results should be regarded as only a qualitative indication of behavior to be expected from these reactions because in no cases can we be sure that surfaces had approached steady state configurations (if these exist), and unknown variables such as trace impurities in the gases or on the surfaces could influence structures and rates. Additional experiments are obviously necessary to characterize any of these systems completely.

It is clear, however, that morphology changes may be as important as surface chemical composition and total surface area in determining the behavior of catalysts. Although there are few systems where reaction rates have been measured on single crystal planes, crystallographic anisotropies of at least an order of magnitude have been reported (*4–7*).

We note that surface morphologies obtained in these experiments should be appropriate for many industrial catalytic reactions. Ammonia oxidation is carried out industrially at conditions very similar to those used here except for higher total pressures and longer operating times. Hydrocarbon and CO oxidation in the automotive converter occurs on supported Pt and Pd crystallites ~ 1 μm in diameter at 1100 K. While we have shown that rates of etching and structures produced depend on sphere diameter and gas flow rate, it should be possible to scale these results to the crystallite diameters and flow conditions of industrial reactions. If d is less than 1 μm, the crystallite should be a polyhedron and relative areas of planes are not governed by the original sphere as for larger spheres. However, until the crystallite size becomes so small that radius of curvature effects dominate (we observe facet edges to have radii less than 500 Å under most conditions), extrapolations from present conditions should not introduce serious errors in morphologies of smaller spheres. These conditions are actually very "mild" compared to industrial reaction conditions.

We also note that the distribution of orientations obtained from single crystal spheres is appropriate to both single crystal crystallites and to randomly oriented polycrystalline surfaces. Consequently, it should be possible to estimate catalytic reaction rates on real catalysts with fairly high accuracy from plane area distributions (data of Table 1) and rate measurements on the planes which exist. It is also interesting to note that the planes near (111) which possess monatomic steps do not exist for any of these reactions except for very short reaction times.

Additional characterization of surface morphology in these and other reaction systems is clearly needed, and we are currently examining time dependences using *in situ* optical reflectance from spheres. Surface chemical characterization is also important to determine crystallographic variations in surface composition, and scanning Auger microscopy promises to be a valuable tool to examine composition variations on single crystal catalyst spheres.

REFERENCES

1. Moore, A. J. W., *in* "Metal Surfaces" (W. D. Robertson and N. A. Gjostein, Eds.), p. 155. Amer. Soc. for Metals, Metals Park, Ohio, 1963.
2. Rhead, G. E., and Mykura, H., *Acta Met.* **10**, 843 (1962).
3. McCabe, R. W., Pignet T., and Schmidt, L. D., *J. Catal.* **32**, 114 (1974).
4. Bussiere, P., Devore, P., Domanski, B., and Prettre, M., *Proc. Int. Congr. Catal., 2nd, 1960* **2**, 2256 (1961).
5. Leidheiser, H., and Gwathmey, A. T., *J. Amer. Chem. Soc.* **70**, 1200; 1206 (1948).
6. Cunningham, R. E., and Gwathmey, A. T., *in* "Advances in Catalysis" (D. D. Eley, W. G. Frankenburg, V. I. Komarewsky, and P. B. Weisz, Eds.), Vol. 10, p. 57. Academic Press, New York, 1958.
7. Meelheim, R. Y., Cunningham, R. E., Lawless, K. R., Azim, S., Kean, R. H., and Gwathmey, A. T., *Proc. Int. Congr. Catal., 2nd, 1960* **2**, 2005 (1961).
8. Jeschkowski, U., and Menzel, E., *Surface Sci.* **15**, 333 (1968).
9. Pignet, T., Schmidt, L. D., and Jarvis, N. L., *J. Catal.* **31**, 145 (1973).
10. Gillespie, G. R., and Kenson, R. E., *Chem. Tech.*, Oct. (1974).
11. Herring, C., *Phys. Rev.* **82**, 87 (1951).
12. Herring, C., *in* "Structure and Properties of Solid Surfaces" (R. Gomer and C. S. Smith, Eds.), p. 5. Univ. of Chicago Press, Chicago, 1952.
13. Cabrera, N., *Surface Sci.* **2**, 320 (1964).
14. Gibbs, J. W., *Trans. Conn. Acad.* **3**, 345 (1878), reprinted in, "The Collected Works of J.

Willard Gibbs," Vol. 1, Dover, New York, 1961.

15. Nicholas, J. F., *Aust. J. Phys.* **21**, 21 (1968).

16. Mullins, W. W., *Phil. Mag., Ser.* 8, **6**, 1313 (1961).

17. Dreger, L. H., and Margrave, J. L., *J. Phys. Chem.* **64**, 1323 (1960).

18. Nowak, E. J., *Chem. Eng. Sci.* **21**, 19 (1966); **24**, 421 (1969).

19. Hondros, E. D., and Moore, A. J. W., *Acta Met.* **8**, 647 (1960).

20. Blakeley, J. M., and Mykura, H., *Acta Met.* **10**, 565 (1962).

21. Norris, L. F., and Parravano, G., *in* "Reactivity of Solids: Proceedings of the 6th International Symp. On the Reactivity of Solids" (J. W. Mitchell, R. C. DeVries, R. W. Roberts, and P. Cannon, Eds.), p. 149. Wiley Interscience, New York, 1969.

22. Pignet, T., and Schmidt, L. D., *J. Catal.* **40**, 212 (1975).

23. Hiam, L., Wise, H., and Chikins, S., *J. Catal.* **10**, 272 (1968).

24. Löffler, D. G., and Schmidt, L. D., I & EC Fundamentals, to be published.